ELSEVIER

Micron 37 (2006) 52–56

micron

www.elsevier.com/locate/micron

Highly anisotropic distribution of iron nanoparticles within MCM-41 Mesoporous Silica

M. Sergio Moreno[a,*], Matthew Weyland[b], Paul A. Midgley[b], José F. Bengoa[c], Marta V. Cagnoli[c], Norma G. Gallegos[c], Ana M. Alvarez[c], Sergio G. Marchetti[c]

[a]*Materials Department, Centro Atómico Bariloche, 8400 San Carlos de Bariloche, Argentina*
[b]*Department of Materials Science and Metallurgy, University of Cambridge, Pembroke Street, Cambridge CB2 3QZ, UK*
[c]*CINDECA, Fac. Cs. Exactas, Fac. Ingeniería, UNLP, CICBA, CONICET. Calle 47 No 257 (1900) La Plata, Argentina*

Received 14 December 2004; revised 8 April 2005; accepted 15 June 2005

Abstract

Electron microscopy techniques are used to visualize the spatial distribution of iron nanoparticles inside a mesoporous MCM-41 molecular sieve. Direct observation of the iron oxide nanoparticles by STEM-HAADF imaging reveals a highly non-uniform spatial distribution inside the mesopores. These particles are retained in the pores after a reduction treatment unlike the behavior found in other similar systems. It is found that thermal treatments induce changes in its morphology, creating nanowires from particle strings.

Keywords: STEM-HAADF; Mesoporous materials; Catalysis; Fe/MCM-41; Iron oxide nanoparticles

Nanoporous and mesoporous materials, such as molecular sieves, are ideal templates for the synthesis of nanowires and can act as hosts for a wide variety of different nanoparticles. The accommodation of such particles, under different environmental conditions, is useful both for practical applications, for example as high efficiency catalysts, and for the general examination of size-dependent effects. It has become clear that tuning the properties that arise because of spatial confinement depends on the precise control of the size, shape, composition and distribution of nanoscale objects. One such mesoporous molecular sieve is MCM-41, a silica (SiO_2) based system consisting of a two-dimensional (2D) hexagonal array of 1D channels whose diameters can be precisely controlled, between 2 and 10 nm, during synthesis (Beck et al., 1992; Ryoo and Kim, 1995). The ability to produce these silica mesopores with precise dimensions provides a unique opportunity to tailor and study nanoscale structures, especially for producing nanostructured objects at scales (e.g. below 5 nm) smaller than other templates. Nanowires obtained from different methods usually have diameters of tens or hundred nanometers (Xia et al., 2003). In principle, the uniform pore structure of MCM-41 should allow a fine selection of any nanoparticle size distribution. In addition, the size constraints of the mesopores may provide appropriate conditions for the synthesis of 1D materials in the form of nanowires. Given this, it may be possible to control and study the aggregation of nanoparticles inside the channels.

The leading application for such mesoporous materials is in the field of heterogeneous catalysis. For example iron nanoparticles supported in MCM-41 can be used to catalyse the benzylation of benzene with benzyl chloride (Trong On et al., 2003) or for hydrocarbon synthesis (Fischer–Tropsch synthesis) (Alvarez et al., 2002). A typical pore size in MCM-41 is about 2.5 nm and allows a potentially high dispersion of the active sites for catalysis. While there have been a vast work on the incorporation of iron oxide in MCM-41 silica materials by post-synthesis modification (Köhn et al., 2003; Schüth et al., 2001; Stockenhuber et al., 2001; Iwamoto et al., 2000; Stockenhuber et al., 2000; Zhang et al., 2001), the characterization of the iron species is usually carried out using techniques such as XRD, XANES/EXAFS, EPR, Mössbauer and FTIR spectroscopy which provide only indirect information on aspects such as

* Corresponding author. Tel.: +54 294 444 5100; fax: +54 294 444 5299.
E-mail address: smoreno@cab.cnea.gov.ar (M.S. Moreno).

0968-4328/$ - see front matter © 2005 Elsevier Ltd. All rights reserved.
doi:10.1016/j.micron.2005.06.003

their size and location. The use of electron microscopy has been far less extensive. For iron loaded MCM-41 some articles report the use of bright field TEM and the presence of the iron nanoparticles has been inferred from changes in the contrast of the images (Schüth et al., 2001; Iwamoto et al., 2000). This technique has important limitations in its application to MCM sieves as reported previously (Midgley et al., 2004) and as we mention below. In consequence, while it is suggested that these nanoparticles are embedded inside the mesopores (Schüth et al., 2001; Iwamoto et al., 2000) (vastly increasing the active surface area of the catalyst), there has been no direct evidence given that the nanoparticles were incorporated into the pore structure. In order to obtain a suitable active catalyst for the Fischer–Tropsch reaction it is necessary to reduce the iron species, usually introduced into the catalyst in a oxidised state, to metallic iron. The challenge in the synthesis of these catalysts is to introduce Fe nanoparticles inside the pores of the MCM-41 and to preserve their location after the activation process. This increases the active surface area and retains a very narrow particle size distribution, leading to a high selectivity and efficiency in catalysis. The unwanted migration of nanoparticles to external surfaces has been seen in iron–zeolite systems (Lin, 1984). As such it is of great importance to determine unambiguously how metal or oxide particles can be introduced into MCM-41 and how they react to any subsequent reduction reaction. The control of size-dependent effects and the improvement and development of such 'nanocatalysts' requires direct information on the size, chemistry, distribution, location and detailed morphology of the nanoparticles that act as the active catalytic sites. Elucidation of such knowledge will allow the control of key catalytic properties: activity, selectivity and stability. At the same time this opens a route to the creation of 3D nanostructures. The study of such 3D features has been performed recently for a different catalyst system (Pt/Ru-MCM41) (Midgley et al., 2004; Midgley et al., 2002; Midgley et al., 2001).

In this article, we present results of an electron microscopic study on the direct visualization of the spatial distribution of the iron containing particles in Fe/MCM-41 system and its evolution under thermal treatments. We analyse samples corresponding to pre- and post-reduction of the precursor for a range of different metal loading.

The MCM-41 support was prepared according to Ryoo and Kim (1995) and impregnated by incipient wetness with $Fe(NO_3)_3.9H_2O$ aqueous solutions ($pH \cong 0.5$). This leads to solids with final Fe concentrations of 5 and 10 wt% (measured by atomic absorption spectroscopy). After drying in air, the samples were calcined in dry N_2 stream (60 cm^3/min) with a temperature ramped from 298 K at a rate of 0.2 K/min, to a final temperature of 598 K. The specimens were held at this temperature for 1 h. The decomposition of the impregnated iron salt generates hematite particles (Alvarez et al., 2002; Köhn et al., 2003). These precursors were reduced in a dry H_2 flow (120 cm^3/min) with a temperature ramped from 298 K at 0.3 K/min, to 698 K and held at this temperature for 26 h. The reduced iron species were cooled in flowing H_2 down to room temperature. The samples studied by electron microscopy were passivated by replacing the H_2 stream with a He–air mixture with a progressive increase of air content over 7 h.

The iron nanoparticles embedded in MCM-41 were studied using High-Angle Annular Dark-Field (HAADF) Scanning Transmission Electron Microscopy (STEM) and Energy Dispersive X-ray Spectroscopy (EDS) (Treacy and Howie, 1980) in a Tecnai F20 TEM operated at 200 kV, with the specimen at room temperature. The incoherent nature of STEM-HAADF imaging provides images whose intensity is approximately proportional to the square of the atomic number, Z, and to the projected thickness (Midgley et al., 2004; Ozkaya et al., 1999). The simple interpretability of this contrast is a great advantage when attempting to identify the clusters within the channels in mesoporous materials. Especially when compared to bright field TEM, where their visibility also depends on many other complex factors; such as the ratio of the particle size to the thickness of the support, the degree of defocus, the coherency of the electron source and the spherical aberration of the objective lens. The combination of HAADF and EDS should allow the unambiguous correlation between image features and their chemistry. In addition, since MCM-41 is electron-beam sensitive another advantage of STEM-HAADF compared to TEM is the reduced total dose needed to acquire similar data. This sensitivity precludes the study of the iron distribution by means of chemical maps acquired using energy-filtered TEM (EFTEM) because of the higher electron doses needed in this technique. Such intense irradiation leads to transformations in the sample.

Fig. 1 shows STEM-HAADF images of the precursor along the directions parallel (Fig. 1a) and perpendicular to the pore axis (Fig. 1b and c). The contrast reveals the highly ordered hexagonal arrangement of the channels, confirming that the MCM-41 structure was clearly maintained after iron impregnation and calcination. Iron oxide species are shown as brighter features due to their higher average Z than the substrate. EDS spectra were acquired for the individual bright features appearing in the images using STEM probes of about 0.5 nm in diameter. The electron-beam sensitivity of the MCM framework imposes important restrictions on the acquisition conditions for the EDS spectra—the small beam current requires longer acquisition times which in turn demands a high sample and beam stability. We found that a reasonable compromise can be reached with acquisition times of 30 s but even then this leads to spectra with very few counts, as can be seen in the spectra shown in the figures. Selective EDS of individual nanoparticles as shown in Fig. 1d unambiguously identifying these as iron rich. The Cu X-ray peaks arise from the proximity of the grid bars of the copper support grid. At least two different types of positions/morphologies of iron oxide particles are apparent in Fig. 1a. The small round spots in the middle of

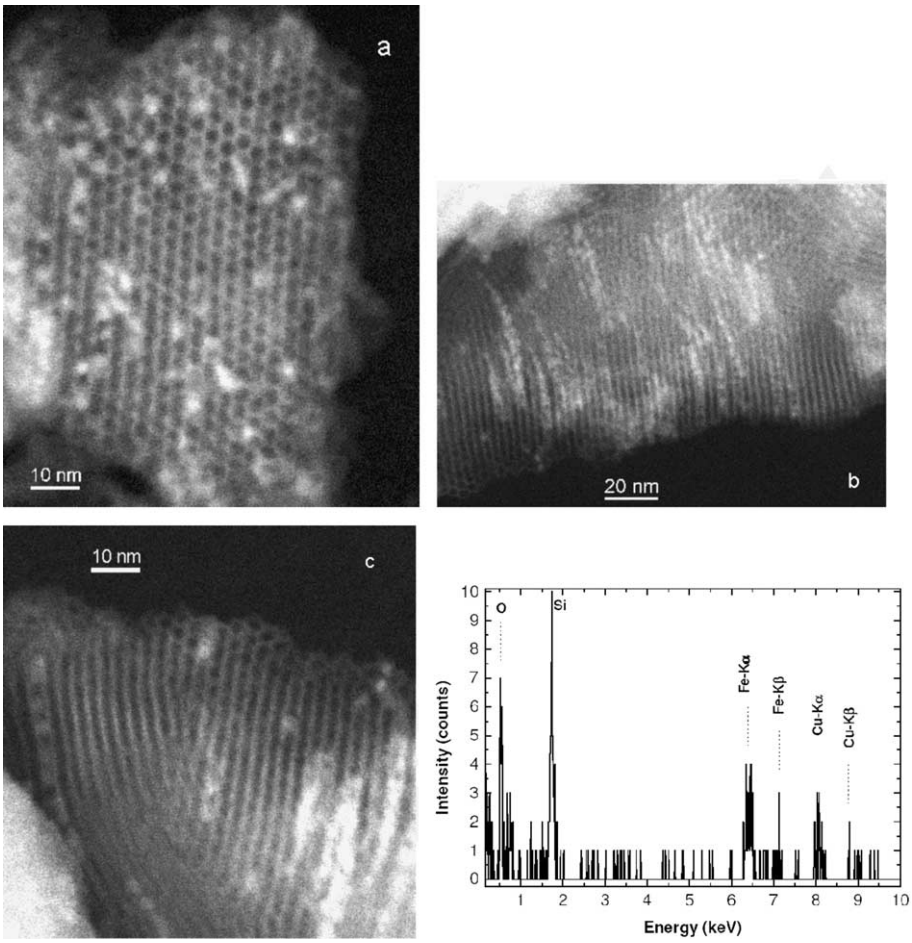

Fig. 1. STEM-HAADF images of the precursor sample along the direction parallel (a) and approximately perpendicular to the pore axis (b)–(c) and the EDS spectrum of a single nanoparticle showing the presence of Fe. It can be observed that not all the pores are filled with iron oxide nanoparticles.

the channels corresponds to iron oxide nanoparticles located inside the pores, demonstrating unambiguously MCM-41 material can effectively stabilize nanoparticles of iron oxide. However, it is evident that not all the channels contain nanoparticles, indeed those that do are a minority, and are not uniformly distributed. Other bright, Fe rich, areas give smeared contrast over more than one pore diameter suggesting iron oxide particles on the external surface. The 'nanowire' like morphology of the bright contrast in Fig. 1b and c clearly confirms that the particles are actually anchored inside the pores, as well as highlighting their inhomogeneous distribution. Examination of such images also indicate that the iron loading has no influence on the iron oxide particles dispersion, the spatial distribution being similar for the sample loaded with 5 and 10 Fe wt%. It has also been observed, in thin regions, that the oxide nanoparticles are individually anchored, that is they have neither coalesced nor sintered together. This inhomogeneous distribution is in disagreement with the 'very homogeneous distribution of the iron' reported by Schüth et al. (2001) by using EDS with a spot size of about 10 nm.

A close inspection of the images reveals that there are no distortions of the pore wall either in the opening of the pore or around the nanoparticles, so in principle, we have to neglect that the inhomogeneous filling is due to a locally enhanced activity because of changes in the curvature. These observations lead to the obvious conclusion that a barrier exists for homogeneous tube filling. One possible such barrier is an inhomogeneous surface chemistry leading to differential wetting of the pores. The inside of the MCM-41 nanopores is essentially hydrophilic due to the presence of sylanols groups. However, it has been demonstrated that sylanol concentration on the pore walls may be inhomogeneous leading to localized hydrophobic zones (Jentys et al., 1999). In regions, there may occur a spontaneous evaporation of the water confined inside the nanotubes (Okamoto et al., 2004). Therefore, after the complete filling of the nanopores with the iron aqueous solution some fraction of the pores will experience this phenomenon, producing the iron salt precipitation without thermal treatment. This would result in an inhomogeneous iron oxide crystal distribution inside the nanopores. While this model provides an explanation for the inhomogeneous spatial distribution it needs to be consistent also with other experimental observations. After impregnation the solid looks dry: that is to say the total volume of impregnating

solution was absorbed into the pores and in the STEM-HAADF images very few iron particles were precipitated on the outside surface of the MCM-41 as in Fig. 1a. A full explanation remains elusive and clearly requires additional experimental work.

These observations reveals that the procedure used in the synthesis gives iron highly dispersed in these materials, anchored inside the pores. Another important feature for many applications is the behaviour of their distribution under thermal treatments. The STEM-HAADF results for the reduced sample (activated catalyst) are shown in Fig. 2. The most striking feature of these images is the appearance of elongated features (nanowire-like or short particle strings) with a variable longitudinal extent but with a lateral dimension approximately the same as the pore size. This elongated morphology was the only type observed for the iron nanoparticles after the reduction treatment. The length distribution of these particles is shown in Fig. 2d. It is peaked at values below 5 nm. A fit with a log-normal distribution gives an average value of 3.8 ± 0.5 nm perhaps an average 'sintering' of two particles. The high intensity of these features strongly indicates that these correspond to nanoparticles anchored inside the channels. We suggest that this elongated morphology arises as a consequence of the reduction treatment; due to the tendency for metallic iron particles to sinter combined with the constraint of the mesopores. This observation acts as indirect proof that the nanoparticles of the precursor oxide are anchored initially inside the channels. Our observations also show that this sintering occurs even at the lower loading; equivalent structures have been observed for both Fe concentrations.

It is of great significance that the particles are not expelled to the external surface after the reducing treatment as happens in iron/zeolite systems under similar reduction treatments (Lin, 1984). This result suggests the suitability of MCM-41 as support for iron catalysts as an alternative to the more established zeolites.

The detail distribution, anchoring (individual or coalescence), composition and morphology in both type of samples should be elucidated by a 3D electron microscopy study such as electrom tomography combined with analytical techniques as EDS (Midgley et al., 2004).

By using STEM-HAADF we have directly observed the spatial distribution of iron nanoparticles within mesoporous MCM-41 silica molecular sieve. It showed that MCM-41 materials can effectively stabilize iron nanoparticles inside the pores. Interestingly, we observed a partial filling of the pores and a highly inhomogeneous distribution of occupied ones. After the reduction treatment the reduced iron species do not migrate to the external surface in contrast to

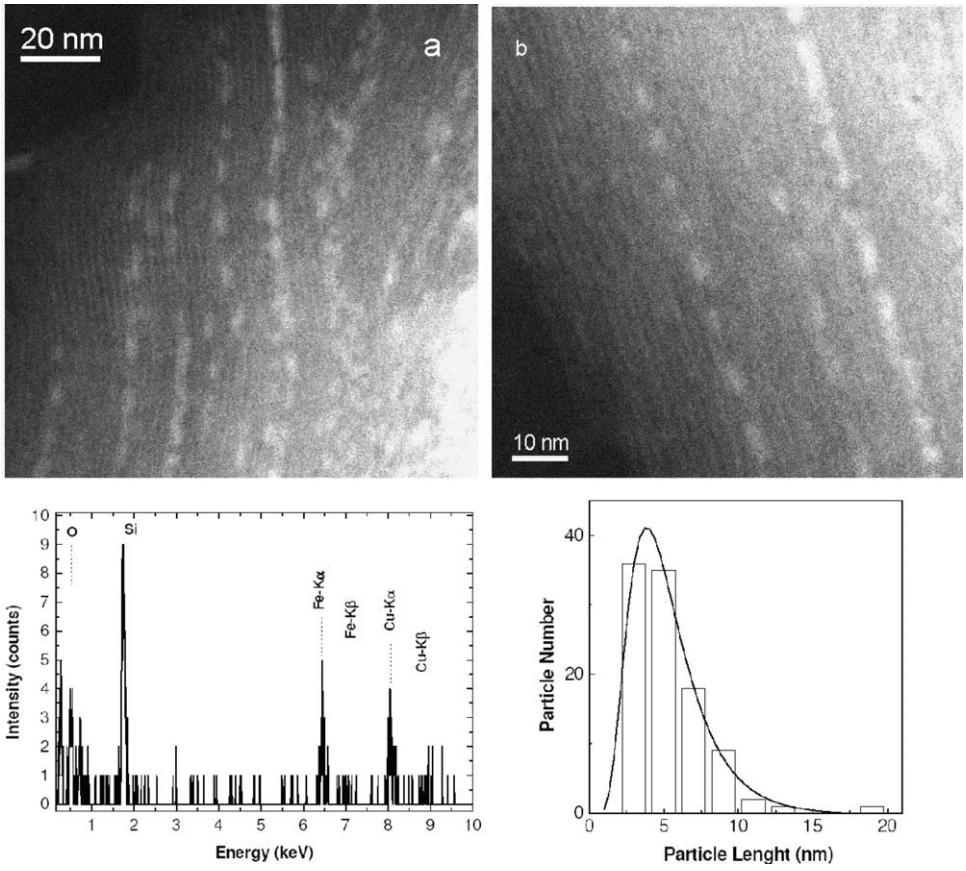

Fig. 2. STEM-HAADF images of the reduced sample (activated catalyst) (a)–(b) and the corresponding EDS spectrum of one of the bright features showing the presence of Fe (c). In (d) is shown the length distribution of the elongated bright features observed in (a)–(b).

the behaviour observed in other iron supported systems, such as iron/zeolite systems. This important finding highlights the advantage of the MCM-41 support for iron catalysts in comparison with zeolites. We have also observed that the morphology of the iron containing particles changes with the thermal treatments from individual nanoparticles to short nanowires or particle strings.

Acknowledgements

M.S. Moreno acknowledges the partial financial support of Consejo Nacional de Investigaciones Científicas y Técnicas (CONICET)-Argentina and the International Atomic Energy Agency (IAEA). PAM and MW thank the Isaac Newton Trust, the British Council, the EPSRC and the Royal Commission for the Exhibition of 1851 for financial support. J.F. Bengoa, M.V. Cagnoli, N.G. Gallegos, A.M. Alvarez and S.G. Marchetti acknowledge support of CONICET, ANPCyT (PICT 14-04315), Comisión de Investigaciones Científicas de la Provincia de Buenos Aires and Universidad Nacional de La Plata, Argentina.

References

Alvarez, A.M., Bengoa, J.F., Cagnoli, M.V., Gallegos, N.G., Yeramián, A. A., Marchetti, S.G., 2002. Fischer-Tropsch synthesis on iron catalysts supported on MCM-41 and MCM-41 modified with Cs. Studies in Surface Science and Catalysis Part A and B 142, 1339–1346.

Beck, J.S., Vartuli, J.C., Roth, W.J., Leonowicz, M.E., Kresge, C.T., Schmitt, K.D., Chu, C.T-W., Olson, D.H., Sheppard, E.W., Mc Cullen, S.B., Higgins, J.B., Schlenker, J.L, 1992. A new family of mesoporous molecular sieves prepared with liquid crystal templates. Journal of the American Chemical Society 114 (27), 10834–10843.

Iwamoto, M., Abe, T., Tachibana, Y., 2000. Control of bandgap of iron oxide through its encapsulation into SiO_2-based mesoporous materials. Journal of Molecular Catalysis A: Chemical 155 (1–2), 143–153.

Jentys, A., Kleestorfer, K., Vinek, H., 1999. Concentration of surface hydroxyl groups on MCM-41. Microporous and Mesoporous Materials 27 (2-3), 321–328.

Köhn, R., Paneva, D., Dimitrov, M., Tsoncheva, T., Mitov, I., Minchev, C., Fröba, M., 2003. Studies on the state of iron oxide nanoparticles in MCM-41 and MCM-48 silica materials. Microporous and Mesoporous Materials 63 (1–3), 125–137 (and references therein).

Lin, T., 1984. Zeolite Supported Iron-Cobalt Catalyst for the Fischer-Tropsch Synthesis; PhD. Northwestern University.

Midgley, P.A., Weyland, M., Thomas, J.M., Johnson, B.F.G., 2001. Z-Contrast tomography: a technique in three-dimensional nanostructural analysis based on Rutherford scattering. Chemical Communications10, 907–908.

Midgley, P.A., Weyland, M., Thomas, J.M., Gai, P.L., Boyes, E.D., 2002. Probing the spatial distribution and morphology of supported nanoparticles using rutherford-scattered electron imaging. Angewandte Chemie International Edition 41 (20), 3804–3807.

Midgley, P.A., Thomas, J.M., Laffont, L., Weyland, M., Raja, R., Johnson, B.F.G., Khimyak, T., 2004. High-resolution scanning transmission electron tomography and elemental analysis of zeptogram quantities of heterogeneous catalyst. Journal of Physical Chemistry 108 (15), 4590–4592.

Okamoto, K., Shook, C.J., Bivona, L., Lee, S.B., English, D.S., 2004. Direct observation of wetting and diffusion in the hydrophobic interior of silica nanotubes. Nano Letters 4 (2), 233–239.

Ozkaya, D., Zhou, W., Thomas, J.M., Midgley, P.A., Keast, V.J., Hermans, S., 1999. High-resolution imaging of nanoparticle bimetallic catalysts supported on mesoporous silica. Catalysis Letters 60 (3), 113–120.

Ryoo, R., Kim, J.M., 1995. Structural order in MCM-41 controlled by shifting silicate polymerization equilibrium. Chemical Communications 7, 711–712.

Schüth, F., Wingen, A., Sauer, J., 2001. Oxide loaded ordered mesoporous oxides for catalytic applications. Microporous and Mesoporous Materials, 44–45 (see also pages 465–476).

Stockenhuber, M., Hudson, M.J., Joyner, R.W., 2000. Preparation, characterization, and unusual reactivity of Fe-MCM-41. Journal of Physical Chemistry B 104 (14), 3370–3374.

Stockenhuber, M., Joyner, R.W., Dixon, J.M., Hudson, M.J., Grubert, G., 2001. Transition metal containing mesoporous silicas - redox properties, structure and catalytic activity. Microporous and Mesoporous Materials, 44–45 (see also pages 367–375).

Treacy, M.M.J., Howie, A., 1980. Contrast effects in the transmission electron microscopy of supported crystalline catalyst particles. Journal of Catalysis 63 (1), 265–269.

Trong On, D., Desplantier-Giscard, D., Danumah, C., Kaliaguine, S., 2003. Perspectives in catalytic applications of mesostructured materials. Applied Catalysis A: General 253 (2), 545–602.

Xia, Y.N., Yang, P.D., Sun, Y.G., Wu, Y.Y., Mayers, B., Gates, B., Yin, Y. D., Kim, F., Yan, Y.Q., 2003. One-dimensional nanostructures: synthesis, characterization and applications. Advanced Materials 15 (5), 353–389.

Zhang, L., Papaefthymiou, G.C., Ying, J.Y., 2001. Synthesis and properties of γ-Fe_2O_3 nanoclusters within mesoporous aluminosilicate matrices. Journal of Physical Chemistry B 105 (31), 7414–7423.